Frontiers of Information Technology & Electronic Engineering
www.jzus.zju.edu.cn; engineering.cae.cn; www.springerlink.com
ISSN 2095-9184 (print); ISSN 2095-9230 (online)
E-mail: jzus@zju.edu.cn

A dual-polarized Fabry–Pérot antenna with high gain and wide bandwidth for millimeter-wave applications*

Qingyi GUO, Hang WONG‡

State Key Laboratory of Terahertz and Millimeter Waves, Department of Electrical Engineering, City University of Hong Kong, Hong Kong 999077, China

E-mail: guo_qingyi@163.com; hang.wong@cityu.edu.hk

Received Sept. 30, 2020; Revision accepted Jan. 20, 2021; Crosschecked Feb. 9, 2021

Abstract: We introduce a dual-polarized (DP) Fabry–Pérot cavity (FPC) antenna operating at the millimeter-wave (mmWave) frequency band with high-gain and wideband characteristics. A DP feeding source and a partially reflective surface (PRS) integrated with a Fresnel zone lens are suggested to realize dual-polarization wave radiation over a wide impedance bandwidth. The feeding source provides vertical and horizontal polarizations while keeping high isolation between the two polarizations. PRS is used to realize Fabry cavity to produce a directive beam radiation. The integrated Fresnel zone rings are introduced for phase correction, leading to a significant gain enhancement for the antenna. For verification, a 60-GHz FPC antenna prototype with DP radiation is designed and fabricated with measurement results. It consists of a feeding source, a PRS integrated with a Fresnel zone lens, a quasi-curved reflector, and four three-dimensional printed supporters. The results illustrate that the peak gains of vertical and horizontal polarizations are 18.4 and 17.6 dBi, respectively. The impedance matching bandwidth for the two polarizations is 14%. The performance ensures that the proposed DP FPC antenna is a promising candidate for the fifth-generation wireless communication systems in the mmWave band.

Key words: Dual polarized; Fabry–Pérot cavity antenna; partially reflective surface integrated with Fresnel zone lens; Millimeter-wave band; High-gain; Wideband;
https://doi.org/10.1631/FITEE.2000514 **CLC number:** TN82

1 Introduction

With the development of emerging wireless systems such as the fifth-generation (5G) communications (Thors et al., 2016), anti-collision radar, high-speed gesture recognition, intelligent sensing network, and millimeter-wave (mmWave) imaging, the operating frequencies of these new systems are likely to be allocated in the mmWave frequency band for its advantages of wide usable frequency bandwidth and large carrying capability. Although mmWave radio can provide a large bandwidth and a high data rate to the systems, its high propagation attenuation in radio signal transmission is its major disadvantage. To compensate for the propagation loss along with millimeter waves, antennas of low-cost and high-gain characteristics are always sought by the communication industry. In previous years, some methods for constructing antennas with a high-gain performance in the mmWave spectrum have been proposed. Examples include antennas involving cavity (Bai et al., 2016), superstrate (Vettikalladi et al., 2009), lens (Imbert et al., 2015), metamaterials (Kaouach, 2016), Yagi–Uda structure (Kramer et al, 2011), and antenna array technologies (Zhu Q et al., 2017; Zhu JF et al., 2018).

In addition to the above-mentioned examples,

‡ Corresponding author

* Project supported by the Research Grant Council of the Hong Kong SAR, China (No. CityU11218318) and the CityU Strategic Research Grant, China (No. SRG-Fd 7005446)

ORCID: Qingyi GUO, https://orcid.org/0000-0001-5546-6471; Hang WONG, https://orcid.org/0000-0002-4009-7009

the Fabry–Pérot cavity (FPC) antenna, formed by placing a partially reflective surface (PRS) above a feeding source integrated reflector, is also a promising way of obtaining a directive beam. In the microwave band, the chessboard-arranged metamaterial superstrate (CAMS) (Zheng et al., 2018), sparse array excitation method (Gardelli et al., 2006), and one-dimensional electromagnetic band gap (EBG) PRS (Leger et al., 2005) are often used for high-gain FPC antenna designs. However, it is difficult for these designs to be scaled to the mmWave band because their complexity in structure makes high-frequency fabrication difficult.

There have been some methods proposed for mmWave high-gain FPC antenna realization. In Vettikalladi et al. (2009), a single-layer superstrate was put on top of 60-GHz patches. This achieves an antenna gain of 14.9 dBi. Using a single-layer frequency selective surface (FSS) (Hosseini et al., 2015a, 2015b; Akbari et al., 2016; Abbou et al., 2017; Attia et al., 2017) as a PRS for an FPC antenna is an alternative method. Introducing a printed ridge-gap waveguide to an FPC antenna (Abbou et al., 2017) can further improve the antenna gain to 15.6 dBi. The example in Chantalat et al. (2008) introduces a metallic EBG structure which can achieve a high directivity of 23.8 dBi at a frequency of 30 GHz. However, the horn-fed approach and profile ($>4\lambda_{30\ \mathrm{GHz}}$) make it heavy and bulky. Moreover, the above-mentioned designs are realized only with linearly polarized radiation.

A dual-polarized (DP) antenna is preferred commonly in communication systems because of its significantly elevated communication capacity and resistance to multipath fading. For DP FPC antenna realization, a DP feeding source is crucial in antenna design. Most DP FPC antennae are designed based on a DP feeding source and a PRS composed of fully symmetric elements (Hamid et al., 2011; Moghadas et al., 2011; Qin PY et al., 2018). In Qin PY et al. (2018), a DP FP antenna was designed using a DP feeding source and a quad-layer PRS. The antenna was demonstrated to yield peak gains for vertical and horizontal polarizations of 14.7 dBi and 15.5 dBi, respectively, with a 1-dB bandwidth of more than 10% for both polarizations. To enhance the realized gain, DP arrays have been proposed to feed the cavity of an FPC antenna (Qin F et al., 2016; Xie et al., 2017). With high-gain sources, an FPC antenna can realize high gain while maintaining DP radiation. However, there are few designs which demonstrate mmWave DP FPC antenna realization with a high gain and a wide bandwidth.

In this study, an mmWave DP FPC antenna is introduced. The proposed antenna is composed of a DP feeding source, a PRS integrated with a Fresnel zone lens (FZL), a quasi-curved reflector, and three-dimensional (3D) printed supporters. The proposed feeding source achieves DP radiation characteristics within a wide frequency range, which ensures wideband performance of the FPC antenna. At the same time, the proposed feeding source can achieve a high isolation level between the two polarizations. The proposed PRS with an integrated Fresnel zone lens provides wave reflection and phase correction in the FP cavity, contributing to a high antenna gain for the antenna. For validation, a fabricated sample of the FPC antenna operating at 60 GHz with the proposed feeding source and PRS is designed and tested. Results show that the antenna has an overlapped impedance bandwidth of 14%. The measured peak gains of horizontal and vertical polarizations are 17.6 and 18.4 dBi, respectively. This antenna finds potential applications in various mmWave wireless systems.

2 Antenna design

2.1 Antenna configuration

The total structure of the proposed antenna is depicted in Fig. 1a. It consists of the proposed DP-feeding source, a PCB-based quasi-curve reflector, and a PRS integrated with an FZL. The DP feeding source consisting of three substrate integrated waveguide (SIW) layers is designed with two transitions, named transitions 1 and 2, for vertical- and horizontal-polarization excitations, respectively. The reflector is composed of four conductor rings with different diameters, as illustrated in Fig. 1d. PRS is designed using a slab with a relatively high dielectric constant. A two-ring FZL is etched on the bottom surface of the PRS to enhance the gain. In this design, the feeding source is fabricated by a Rogers 4003 substrate with a loss tangent of 0.004, a thickness of 0.508 mm, and a relative permittivity of 3.38. The quasi-curve reflector is designed using a Rogers

Duriod 5880 substrate with a relative permittivity of 2.2, a thickness of 0.787 mm, and a loss tangent of 0.004 (Li and Luk, 2015). The PRS substrate is Rogers Duroid 6006 with a loss tangent of 0.025 (@10 GHz), a thickness of 0.63 mm, and a relative dielectric constant of 6.15. Herein, we set the distance between PRS and the feeding source at 1.5λ (where λ represents the wavelength in free space) at 60 GHz (Wu and Luk, 2017). The initial diameter of the PRS is set at 6λ and the initial thickness of the substrate is close to a quarter-wavelength (in substrate) to provide the maximum reflectivity (Wu and Luk, 2017). All substrates are fixed using four plastic screws. The distance between the PRS and the feeding source is fixed using four 3D printed supporters. Parameters of the proposed antenna are summarized in Table 1.

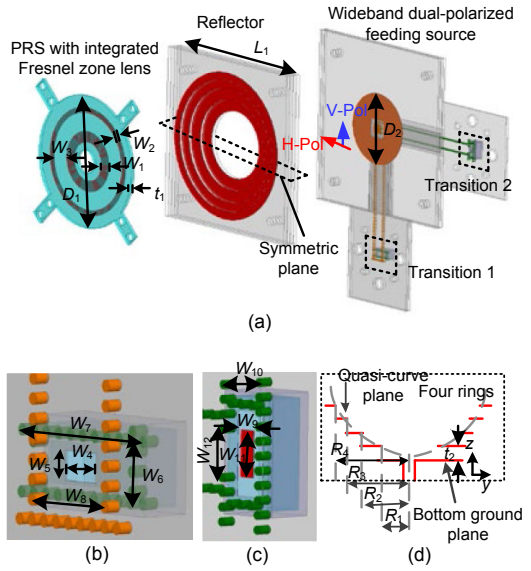

Fig. 1 Total structure of the proposed antenna (a), the structure of transitions 1 (b) and 2 (c), and the structure of the reflector (d) (PRS: partially reflective surface)

Table 1 Detailed dimensions of the antenna structure in Fig. 1 (unit: mm)

Para.	Value	Para.	Value	Para.	Value
L_1	41	W_1	2.54	W_2	1.25
W_3	4.51	W_4	1.25	W_5	0.75
W_6	1.54	W_7	4.10	W_8	3.00
W_9	0.60	W_{10}	1.70	W_{11}	1.60
W_{12}	1.65	D_1	32.0	D_2	17.1
R_1	8.17	R_2	11.00	R_3	13.81
R_4	15.88	t_1	0.630	t_2	0.787

The purpose of the design is to achieve a DP FPC antenna in the mmWave frequency band with high-gain and wideband characteristics. The feeding source generates DP radiation within a wide frequency range. We introduce its design first. Then we conduct analysis on the PRS which contributes to the high-gain performance of the proposed antenna.

2.2 Dual-polarized feeding source design

A feeding source based on an SIW structure is a good candidate for an FPC antenna design owing to its planar configuration which is easy to integrate with other circuitries. Hence, we design an SIW-fed DP source antenna (Fig. 2). It consists of three SIW layers. The radiator is a magnetic-electric dipole (Sun and Wong, 2020) with a symmetric structure along the x and y axes. It is surrounded by a cavity with the dimension of L_{c1}, formed by an SIW structure (denoted in yellow). The antenna is excited by feeding slots. Slot 1 is etched on the top metallic surface of layer 3. Slots 2 and 3 are etched on the top metallic surface of layer 2. Slot 3 is used to couple the wave from port 1 to the radiator, which can generate the radiation with the electric field lying along the *xoz* coordinate plane, designed as the vertical-polarized radiation (V-P).

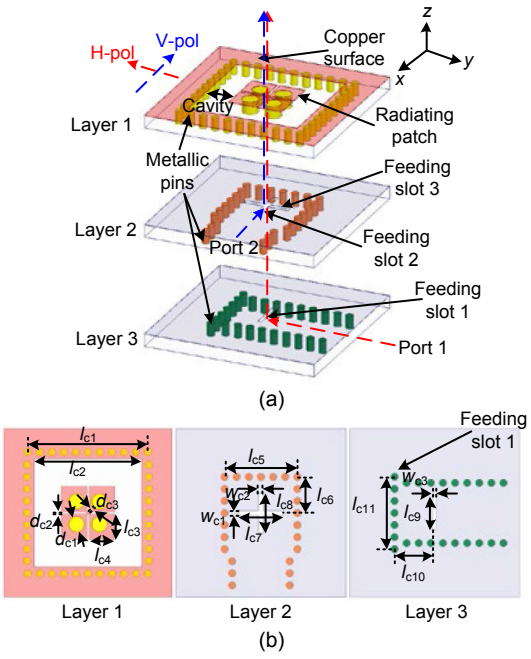

Fig. 2 Configuration of the proposed dual-polarized feeding source (a) and the layer-by-layer demonstration of the source antenna (b) (References to color refer to the online version of this figure)

Slots 1 and 2 are used to couple the wave from port 1 to the radiator through layer 2. This can generate the radiation with the electric field lying on the *yoz* plane, called "horizontal-polarized radiation (H-P)." Detailed views of each SIW layer and related dimensions are illustrated in Fig. 2b and Table 2, respectively.

Table 2 Parameters of the proposed dual-polarized feeding source (unit: mm)

Para.	Value	Para.	Value	Para.	Value
L_{c1}	5.00	L_{c2}	4.50	L_{c3}	1.05
L_{c4}	1.05	L_{c5}	3.00	L_{c6}	1.50
L_{c7}	1.85	L_{c8}	1.65	L_{c9}	1.38
L_{c10}	1.65	L_{c11}	3.00	W_{c1}	0.20
W_{c2}	0.20	d_{c1}	1.30	d_{c2}	0.10
d_{c3}	0.07				

The simulated radiation patterns of the two polarizations at 60 GHz are shown in Fig. 3. As can be seen, broadside radiation directions are obtained at a −20 dB cross-polarization level for the two polarizations. Stable radiation patterns are realized within the whole operating bandwidth (here we show the patterns at only 60 GHz for brevity). The simulated reflection coefficients and the isolation of the two ports are illustrated in Fig. 4. It can be seen that the proposed feeding source yields an operating bandwidth of 16.4% from 56 GHz to 66 GHz. The transmission parameter S_{21} is −50 dB, which means that a good isolation level between two ports is obtained.

The realized gains of the two polarizations are illustrated in Fig. 5. For vertical polarization, a peak of 8.3 dBi realized gain is achieved. For horizontal polarization, the peak gain is 8 dBi. The difference between the gains of the two polarizations is lower than 0.5 dB within the bandwidth from 56 GHz to 66 GHz.

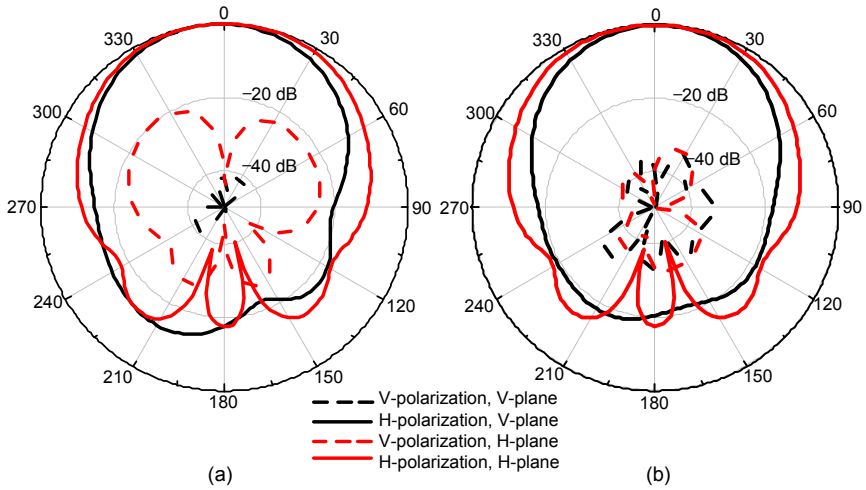

Fig. 3 Radiation patterns at 60 GHz of V-polarization (a) and H-polarization (b) (References to color refer to the online version of this figure)

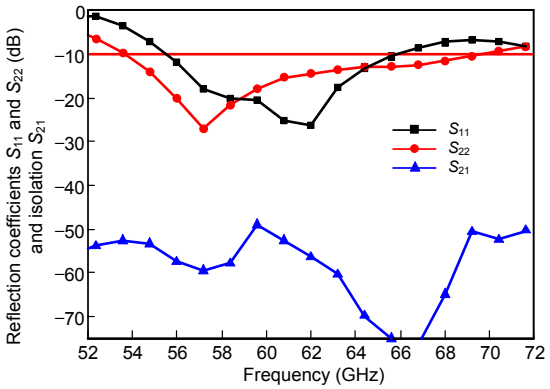

Fig. 4 Reflection configurations and isolation of the two polarizations

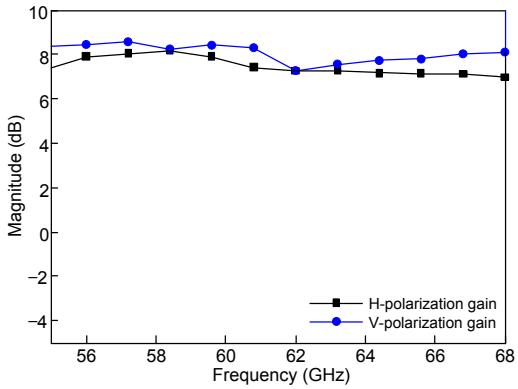

Fig. 5 Realized gain of the two polarizations

Combined with the quasi-curve reflector, wide impedance and gain bandwidths can be obtained. The four concentric strip rings in multilayer substrates make a quasi-parabolic plane, which is used to excite different Laguerre-Gaussian beam modes in the cavity. Hence, a wide gain bandwidth can be obtained (Wu and Luk, 2017). It should be mentioned that the proposed reflector and PRS are both circular. To investigate the effect of shapes of the reflector and the PRS on the gain of the proposed antenna, Fig. 6 illustrates the gain performances for different shapes of the reflector and PRS (called "strategies 1 to 4"). The rectangular shapes of the reflector and PRS result in gain decrease compared with the antenna with the proposed circular reflector and PRS. This is because the top angles of the PRS and reflector will bring discontinuity to the transmitted and reflected waves. Hence, the proposed antenna structure using the circular reflector and the PRS has the highest efficiency in increasing the antenna gain, as depicted in Fig. 7.

2.3 Analysis on the partially reflective surface with an integrated Fresnel zone lens

A conventional FPC antenna (Fig 8a) can generate a directive beam in the broadside direction. However, the antenna gain is limited by the loss from

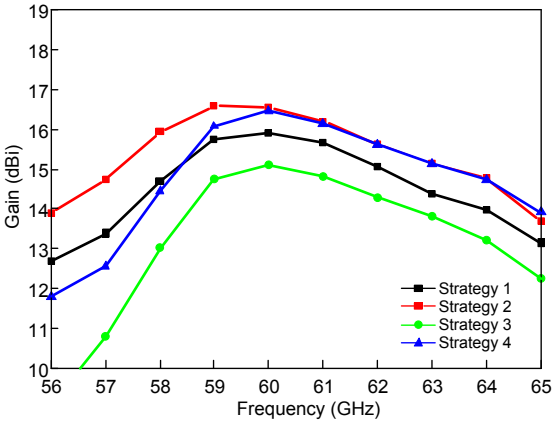

Fig. 7 Realized vertical gain of the antenna with different strategies

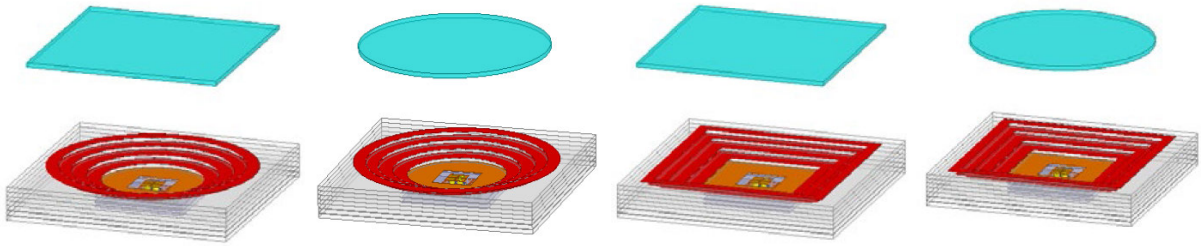

Fig. 6 Proposed antenna with different combination strategies of the reflector and PRS: (a) strategy 1 (circular curve surface and rectangle lens); (b) strategy 2 (circular curve surface and circular lens); (c) strategy 3 (rectangle curve surface and rectangle lens); (d) strategy 4 (rectangle curve surface and circular lens)

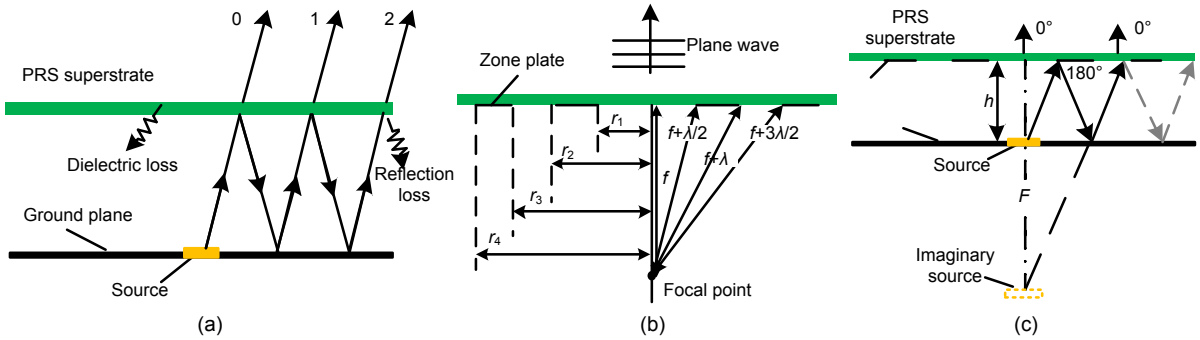

Fig. 8 Configurations of the traditional FPC antenna prototype (a), the transmission FZL (b), and the proposed FPC antenna using an FZL-integrated PRS (c)

FPC: Fabry–Pérot cavity; FZL: Fresnel zone lens; PRS: partially reflective surface

multiple reflection of the wave in the FPC and inaccurate inbound phase distribution on the top surface of the PRS. In our design, we suggest applying an FZL integrated PRS to improve the gain of the FPC antenna. It can achieve accurate in-phase distribution on the top surface of PRS, contributing to a significant gain enhancement.

Generally, an FZL antenna consists of a feeding antenna and several concentric metallic rings. The feeding source locates in the focal point of FZL (Fig. 8b). In-phase waves propagated from the source can transmit through the region without metallic rings. Out-of-phase waves are reflected by the region with metallic rings. Combined with these two conditions, the in-phase wave distribution on the top surface of FZL can be realized, leading to a directive beam radiation. Note that the condition of phase control is determined by f, which is the focal length of FZL, and that r_n is the radius of each zone. r_n can be found from Karimkashi and Kishk (2011):

$$r_n=\sqrt{nf\lambda+\left(\frac{n\lambda}{2}\right)^2}, \tag{1}$$

where n is an integer and λ is the wavelength. The width of each ring is r_n-r_{n-1}. According to the equation, we can find that the width (r_n-r_{n-1}) gradually decreases with the increase in the width of the ring. It means that r_2-r_1 is larger than r_3-r_4 in this design.

Based on the operating scheme of FPC and FZL antennas, we introduce an FZL-integrated PRS to realize high-gain FPC antenna. The design principle of the proposed antenna is shown in Fig. 8c. FZL is printed on the bottom surface of a PRS to form an integrated structure. The operating principle of the proposed antenna is described as follows: In Fig. 8c, considering that a feeding antenna radiates at the center of the ground plane, two conditions of the wave within FPC can occur. In the first condition, in-phase waves transmit through the FZL-integrated PRS within the non-metal region. The outcome of the wave front from FZL contributes to the directive beam radiation in the broadside direction because of the superposition of in-phased wave radiations at the non-metal regions of FZL. The second condition is that the waves can be reflected because of the high dielectric constant of PRS and the metallic rings of FZL. The reflected waves generate FPC reflection between the PRS and the ground plane. Some reflected waves go back to the FZL apertures again and radiate out. Combining the above-mentioned conditions, the proposed FPC antenna can achieve a significant gain enhancement using the PRS integrated with an FZL. The gain enhancement is illustrated in Fig. 9.

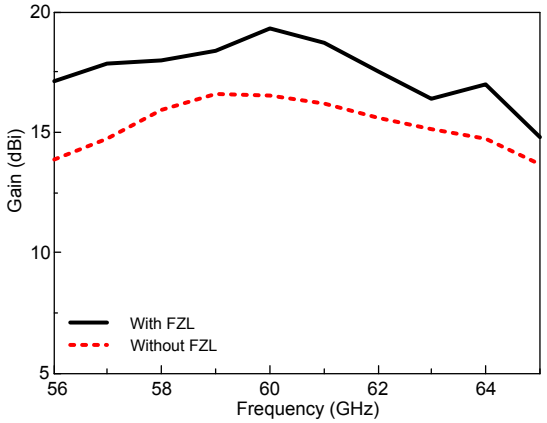

Fig. 9 Simulated antenna gains for the proposed antenna with/without the proposed Fresnel zone lens (FZL)

At the same time, a more uniform phased distribution can lead to a better side lobe level. As a demonstration, Fig. 10 illustrates the phased distribution on PRS with/without FZP and the related radiation patterns. As can be seen from Fig. 10c, the side lobe level on PRS with FZP is lower than that without FZP.

3 Measurement results

Based on the analysis above, an FPC antenna prototype is designed, fabricated, and measured. The fabricated antenna is illustrated in the insertion of Fig. 11a. The size of the antenna is 41 mm×41 mm ×11.4 mm.

The simulated and measured reflection coefficients of the two polarizations are also shown in Fig. 11a. From the measured reflection coefficient curves, we can obtain that the overlapped operating bandwidths of the two polarizations are $|S_{11}|$=14% and $|S_{22}|\leq-10$ dB. From the simulated and measured antenna gains in Fig. 11b, we can observe that the realized gain of horizontal polarization is 17.6 dBi with a

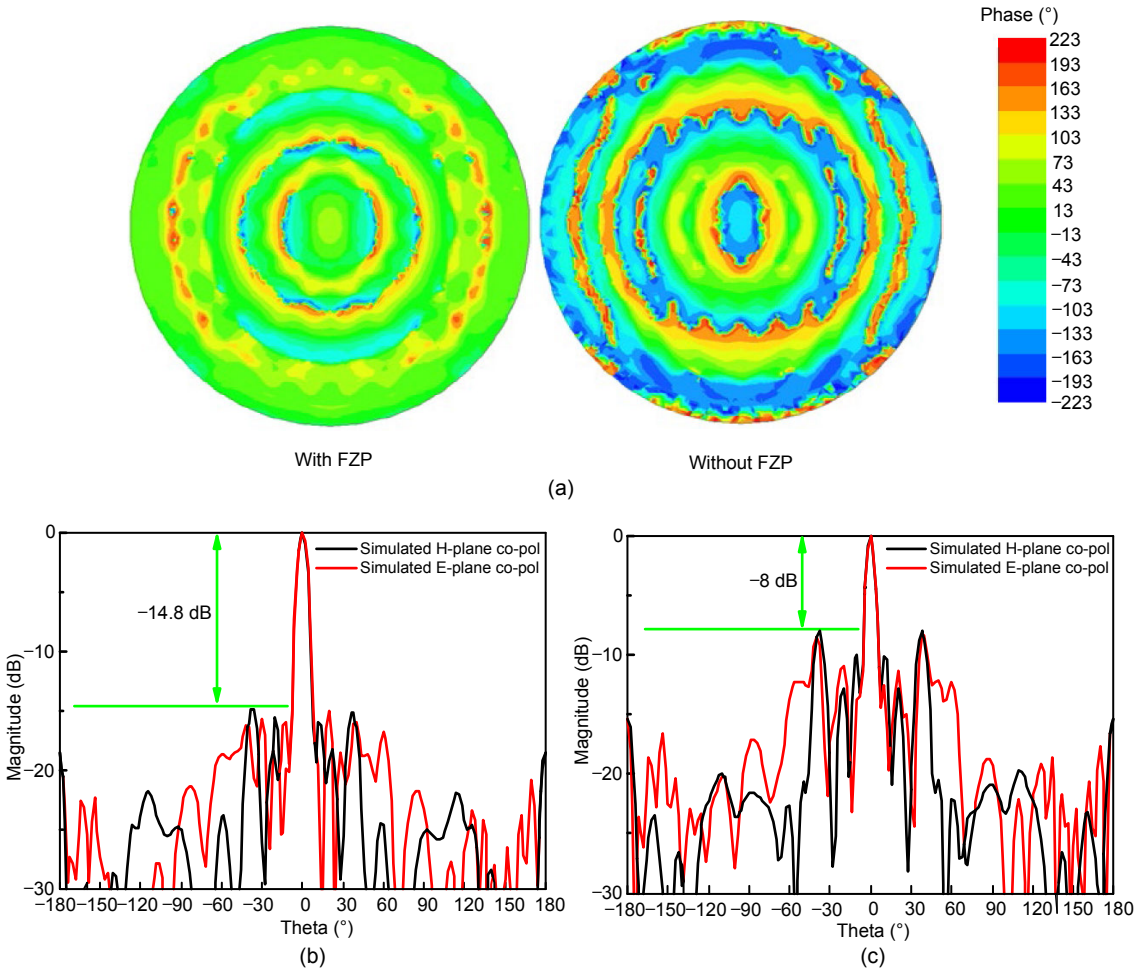

Fig. 10 Phase distributions of the electric field on the top surface of the partially reflective surface for antenna with/without the proposed Fresnel zone lens (FZL) (a) and the radiation patterns at 60 GHz of antenna with (b) and without (c) FZL

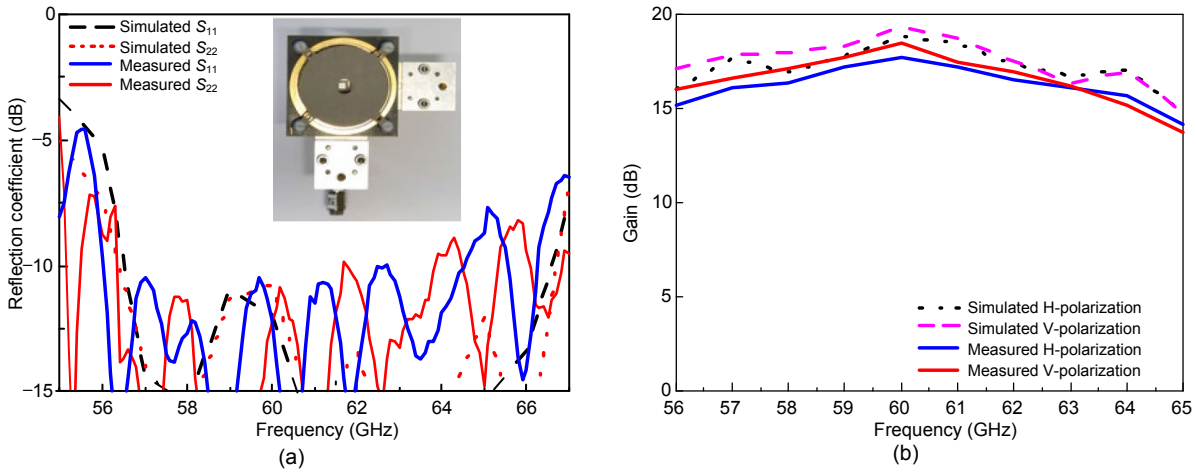

Fig. 11 Simulated and measured reflection coefficients (a) and antenna gains (b) (Insertion in (a) is the fabricated antenna prototype)

variation of 2.4 dB over the operating bandwidth. The measured peak gain of vertical polarization is 18.4 dBi with a variation of 3 dB. The difference between the gains of the two polarizations is less than 1 dB. The differences between the simulation and measurement results may come from the extended SIW transition to the metallic adaptor for the preparation of measurement.

The simulated and measured transmission coefficients of the two ports are depicted in Fig. 12. A transmission level of −40 dB is realized. It means that a good isolation between two polarizations is achieved.

The simulated and measured radiation patterns for the antenna operating at 57, 60, and 64 GHz when port 1 is excited (V-polarization) are illustrated in Fig. 13. The main beams of the E- and H-plane point towards a broadside direction. The radiation patterns at three frequency points within the operating bandwidth are stable and symmetric. The simulated and measured radiation patterns for the antenna operating at 57, 60, and 64 GHz when port 2 is excited (H-polarization) are illustrated in Fig. 14. The patterns of H-polarization are similar to those of V-polarization. The difference between the simulation

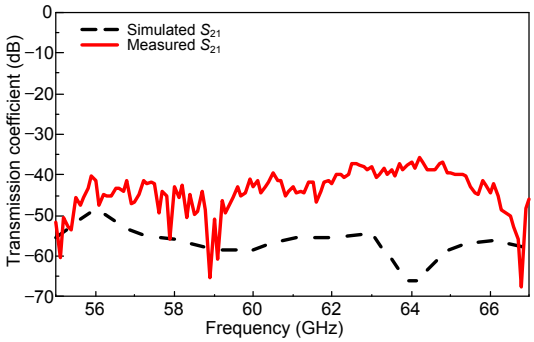

Fig. 12 Simulated and measured transmission coefficients between two polarizations

and measurement results is due mainly to the influence of the fixtures, screws, and feeding setup including waveguide adapters. From the measurement results in Fig. 15, it can be seen that a cross-polarization level of −20 dB is achieved. This means that the energy of cross-polarization of the proposed antenna is low.

4 Conclusions

In this paper, we have presented a design of a high-gain mmWave FPC antenna. The proposed

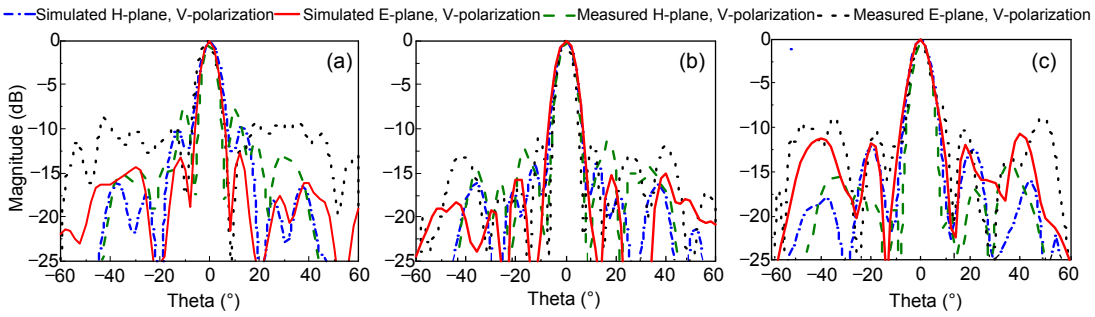

Fig. 13 Simulated and measured radiation patterns for antenna operating at *f*=57 GHz (a), 60 GHz (b), and 64 GHz (c) when port 1 is excited (V-polarization)

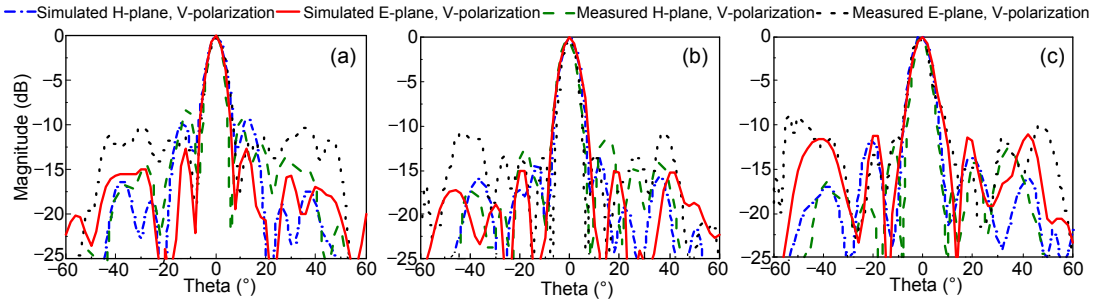

Fig. 14 Simulated and measured radiation patterns for antenna operating at *f*=57 GHz (a), 60 GHz (b), and 64 GHz (c) when port 2 is excited (H-polarization)

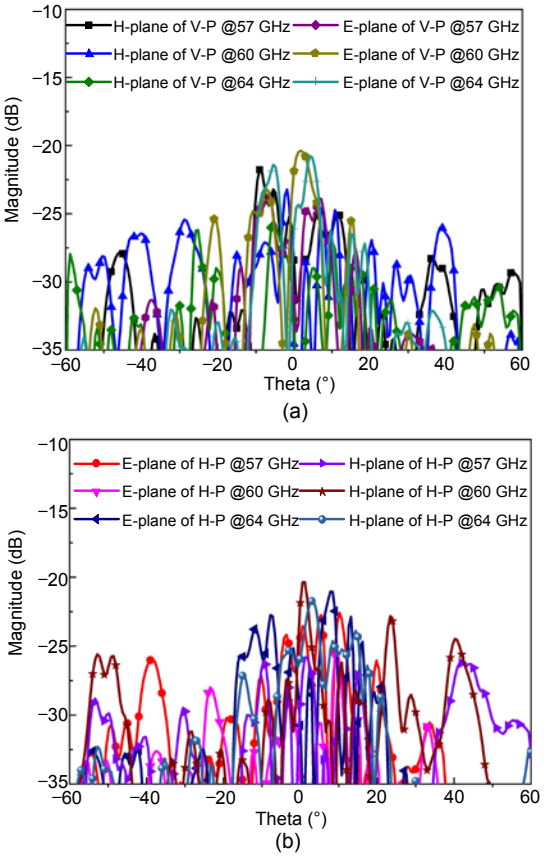

Fig. 15 Measured cross-polarizations of V-polarization (V-P) (a) and H-polarization (H-P) (b) at different frequency points

antenna demonstrates a directive beam for DP radiations. A DP feeding source and a PRS integrated with an FZL have been proposed. This work demonstrates the implementation of a DP FPC antenna with a high-gain and wideband performance while maintaining high isolation for two polarizations. Detailed analysis has been carried out to characterize the proposed methodology and the design principle of the antenna. The antenna obtains the maximum gains of 18.4 dBi and 17.6 dBi, for vertical and horizontal polarizations, respectively, and yields an impedance bandwidth of 14% with a high isolation of −40 dB. This antenna will find potential applications in various wireless mmWave communication systems.

Contributors

Qingyi GUO designed the research. Hang WONG guided the research. Qingyi GUO processed the data and drafted the manuscript. Hang WONG helped organize the manuscript. Qingyi GUO and Hang WONG revised and finalized the paper.

Compliance with ethics guidelines

Qingyi GUO and Hang WONG declare that they have no conflict of interest.

References

Abbou D, Vuong TP, Touhami R, et al., 2017. High-gain wideband partially reflecting surface antenna for 60 GHz systems. *IEEE Antenn Wirel Propag Lett*, 16:2704-2707. https://doi.org/10.1109/LAWP.2017.2742862

Akbari M, Gupta S, Farahani M, et al., 2016. Gain enhancement of circularly polarized dielectric resonator antenna based on FSS superstrate for MMW applications. *IEEE Trans Antenn Propag*, 64(12):5542-5546. https://doi.org/10.1109/TAP.2016.2623655

Attia H, Abdelghani ML, Denidni TA, 2017. Wideband and high-gain millimeter-wave antenna based on FSS Fabry–Perot cavity. *IEEE Trans Antenn Propag*, 65(10): 5589-5594. https://doi.org/10.1109/TAP.2017.2742550

Bai X, Qu SW, Yang SW, et al., 2016. Millimeter-wave circularly polarized tapered-elliptical cavity antenna with wide axial-ratio beamwidth. *IEEE Trans Antenn Propag*, 64(2):811-814. https://doi.org/10.1109/TAP.2015.2507171

Chantalat R, Menudier C, Thevenot M, et al., 2008. Enhanced EBG resonator antenna as feed of a reflector antenna in the Ka band. *IEEE Antenn Wirel Propag Lett*, 7:349-353. https://doi.org/10.1109/LAWP.2008.921343

Gardelli R, Albani M, Capolino F, 2006. Array thinning by using antennas in a Fabry–Perot cavity for gain enhancement. *IEEE Trans Antenn Propag*, 54(7):1979-1990. https://doi.org/10.1109/TAP.2006.877172

Hamid M, Mojgan D, Pedram M, 2011. A dual-band high-gain resonator antenna with orthogonal polarizations. *IEEE Antenn Wirel Propag Lett*, 10:1220-1223. https://doi.org/ 10.1109/LAWP.2011.2173454

Hosseini A, Capolino F, de Flaviis F, 2015a. Gain enhancement of a V-band antenna using a Fabry-Pérot cavity with a self-sustained all-metal cap with FSS. *IEEE Trans Antenn Propag*, 63(3):909-921. https://doi.org/10.1109/TAP.2014.2386358

Hosseini A, de Flaviis F, Capolino F, 2015b. A 60 GHz simple-to-fabricate single-layer planar Fabry–Pérot cavity antenna. *IET Microw Antenn Propag*, 9(4):313-318. https://doi.org/10.1049/iet-map.2014.0408

Imbert M, Papió A, de Flaviis F, et al., 2015. Design and performance evaluation of a dielectric flat lens antenna for millimeter-wave applications. *IEEE Antenn Wirel Propag Lett*, 14:342-345. https://doi.org/10.1109/LAWP.2014.2363596

Kaouach H, 2016. Design and characterization of circularly polarized discrete lens antennas in 60-GHz band. *IEEE Antenn Wirel Propag Lett*, 15:1200-1203. https://doi.org/10.1109/LAWP.2015.2499703

Karimkashi S, Kishk AA, 2011. Focusing properties of Fresnel zone plate lens antennas in the near-field region. *IEEE Trans Antenn Propag*, 59(5):1481-1487.

https://doi.org/10.1109/TAP.2011.2123069

Kramer O, Djerafi T, Wu K, 2011. Very small footprint 60 GHz stacked Yagi antenna array. *IEEE Trans Antenn Propag*, 59(9):3204-3210. https://doi.org/10.1109/TAP.2011.2161562

Leger L, Monediere T, Jecko B, 2005. Enhancement of gain and radiation bandwidth for a planar 1-D EBG antenna. *IEEE Microw Wirel Compon Lett*, 15(9):573-575. https://doi.org/10.1109/LMWC.2005.855373

Li MJ, Luk KM, 2015. Wideband magneto-electric dipole antenna for 60-GHz millimeter-wave communications. *IEEE Trans Antenn Propag*, 63(7):3276-3279. https://doi.org/10.1109/TAP.2015.2425418

Moghadas H, Daneshmand M, Mousavi P, 2011. A dual-band high-gain resonant cavity antenna with orthogonal polarizations. *IEEE Antenn Wirel Propag Lett*, 10:1220-1223. https://doi.org/10.1109/LAWP.2011.2173454.

Qin F, Gao SS, Luo Q, et al., 2016. A simple low-cost shared-aperture dual-band dual-polarized high-gain antenna for synthetic aperture radars. *IEEE Trans Antenn Propag*, 64(7):2914-2922. https://doi.org/10.1109/TAP.2016.2559526

Qin PY, Ji LY, Chen SL, et al., 2018. Dual-polarized wideband Fabry–Perot antenna with quad-layer partially reflective surface. *IEEE Antenn Wirel Propag Lett*, 17(4):551-554. https://doi.org/10.1109/LAWP.2018.2802439

Sun GH, Wong H, 2020. A planar millimeter-wave antenna array with a pillbox-distributed network. *IEEE Trans Antenn Propag*, 68(5):3664-3672. https://doi.org/10.1109/TAP.2020.2963931

Thors B, Colombi D, Ying ZN, et al., 2016. Exposure to RF EMF from array antennas in 5G mobile communication equipment. *IEEE Access*, 4:7469-7478. https://doi.org/10.1109/ACCESS.2016.2601145

Vettikalladi H, Lafond O, Himdi M, 2009. High-efficient and high-gain superstrate antenna for 60-GHz indoor communication. *IEEE Antenn Wirel Propag Lett*, 8:1422-1425. https://doi.org/10.1109/LAWP.2010.2040570

Wu F, Luk KM, 2017. Wideband high-gain open resonator antenna using a spherically modified, second-order cavity. *IEEE Trans Antenn Propag*, 65(4):2112-2116. https://doi.org/10.1109/TAP.2016.2647700

Xie P, Wang GM, Li HP, et al., 2017. A dual-polarized two-dimensional beam-steering Fabry–Pérot cavity antenna with a reconfigurable partially reflecting surface. *IEEE Antenn Wirel Propag Lett*, 16:2370-2374. https://doi.org/10.1109/LAWP.2017.2718567

Zheng YJ, Gao J, Zhou YL, et al., 2018. Wideband gain enhancement and RCS reduction of Fabry–Perot resonator antenna with chessboard arranged metamaterial superstrate. *IEEE Trans Antenn Propag*, 66(2):590-599. https://doi.org/10.1109/TAP.2017.2780896

Zhu JF, Liao SW, Yang Y, et al., 2018. 60 GHz dual-circularly polarized planar aperture antenna and array. *IEEE Trans Antenn Propag*, 66(2):1014-1019. https://doi.org/10.1109/TAP.2017.2784445

Zhu Q, Ng KB, Chan CH, 2017. Printed circularly polarized spiral antenna array for millimeter-wave applications. *IEEE Trans Antenn Propag*, 65(2):636-643. https://doi.org/10.1109/TAP.2016.2640019